Inorg. Chem. **2008**, *47*, 7813−7823

General Synthesis and Phase Control of Metal Molybdate Hydrates $MMoO_4 \cdot nH_2O$ (M = Co, Ni, Mn, n = 0, 3/4, 1) Nano/Microcrystals by a Hydrothermal Approach: Magnetic, Photocatalytic, and Electrochemical Properties

Yi Ding, Yong Wan, Yu-Lin Min, Wei Zhang, and Shu-Hong Yu*

Division of Nanomaterials & Chemistry, Hefei National Laboratory for Physical Sciences at Microscale, Structural Research Laboratory of CAS, Department of Chemistry, University of Science and Technology of China, Hefei 230026, P.R. China.

Received May 1, 2008

Different phases and morphologies of molybdate hydrates $MMoO_4 \cdot nH_2O$ (M = Co, Ni, Mn, n = 0, 3/4, 1) nano/microcrystals, which include $NiMoO_4 \cdot H_2O$ microflowers, $MnMoO_4 \cdot H_2O$ microparallelogram plates, and $CoMoO_4 \cdot 3/4H_2O$ microrods, can be selectively synthesized by a hydrothermal process. The pH and reaction temperature have a crucial influence on the synthesis and shape evolution of the final products. Uniform $CoMoO_4 \cdot 3/4H_2O$ and $NiMoO_4 \cdot H_2O$ nanorod bundles can be produced by a hydrothermal process with the assistance of PEG-400. The calcination of $CoMoO_4 \cdot 3/4H_2O$ and $NiMoO_4 \cdot H_2O$ at 500 and 550 °C, respectively, allows the formation of monoclinic β-$CoMoO_4$ and α-$NiMoO_4$. The antiferromagnetic property of $MnMoO_4 \cdot H_2O$, $MnMoO_4$, and $CoMoO_4 \cdot 3/4H_2O$ has been studied for the first time. The photocatalytic activity of metal molybdate particles with different morphologies has been tested by degradation of *acid fuchsine* under visible light. Electrochemical performances of $MMoO_4$ (M = Ni, Co) nanorod bundles and $MnMoO_4$ microrods have been evaluated.

1. Introduction

Metal tungstates and molybdates, two important families of inorganic materials, have a potential application in various fields, such as catalysis,[1] magnetic properties,[2] humidity sensors,[3] and photoluminescence.[4] Tungstates and molybdates with relatively large bivalent cations (ionic radius > 0.99 Å such as Ca, Ba, Pb, Sr) exist in the form of the so-called scheelite structure, where the molybdenum (or tungsten) atom adopts a tetrahedral coordination.[5]

Tungstates and molybdates with smaller bivalent cations (ionic radius < 0.77 Å, for example, Fe, Mn, Co, Ni, Mg, Zn) belong to the wolframite structure, where the tungsten (or molybdenum) atom adopts an overall 6-fold coordination.[6] Most previous approaches to obtain molybdates or tungstates need high temperature and harsh reaction conditions, such as a solid-state reaction at 1000 °C,[7] and the sol−gel method.[8] Soft chemistry routes have already been demonstrated to controllably synthesize this family of materials, for example, one-dimensional and two-dimensional $CdWO_4$ nanocrystals with an improved fluorescence behavior by polymer-controlled mineralization reactions.[9] Uniform, single crystalline $BaWO_4$ nanowires and nanobelts with high aspect-ratio were synthesized using a reversed micelle templating method.[10] Recently, our group has reported a general method for the hydrothermal synthesis of a family of tungstate and molybdate nanorods/nanowires and three-dimensional structures such as MWO_4 (M = Zn, Mn, Fe),

* To whom correspondence should be addressed. E-mail: shyu@ustc.edu.cn. Fax: + 86 551 3603040.

(1) Adeira, L. M.; Portela, M. F.; Mazzocchia, C. *Catal. Rev. - Sci. Eng.* **2004**, *46*, 53.
(2) Livage, C.; Hynaux, A.; Marrot, J.; Nogues, M.; Férey, G. *J. Mater. Chem.* **2002**, *12*, 1423.
(3) Sears, W. M. *Sens. Actuators, B: Chem.* **2000**, *67*, 161.
(4) Liu, B.; Yu, S. H.; Li, L. J.; Zhang, Q.; Jiang, K. *Angew. Chem., Int. Ed.* **2004**, *43*, 4745.
(5) Hyde, B. G.; Andersson, S.; *Inorganic Crystal Structure.*; Wiley: New York, 1989.
(6) Young, A. P.; Schwartz, C. H. *Science* **1963**, *141*, 348.
(7) Swanson, H. E.; Morris, M. C.; Stinchfield, R. P.; Evans, E. H. *NBS Monogr. (U.S.)* **1963**, *25*, 24.
(8) Bonanni, M.; Spanhel, L.; Lerch, M.; Fuglein, E.; Muller, G. *Chem. Mater.* **1998**, *10*, 304.
(9) Yu, S. H.; Antonietti, M.; Cölfen, H.; Giersig, M. *Angew. Chem., Int. Ed.* **2002**, *41*, 2356.
(10) (a) Kwan, S.; Kim, F.; Akana, J.; Yang, P. D. *Chem. Commun.* **2001**, *5*, 447. (b) Shi, H. T.; Wang, X. H.; Zhao, N. N.; Qi, L. M.; Ma, J. M. *J. Phys. Chem. B* **2006**, *110*, 748.

10.1021/ic8007975 CCC: $40.75
Published on Web 08/06/2008

Bi_2WO_6, Ag_2WO_4, $Ag_2W_2O_7$, $Ag_6Mo_{10}O_{33}$, and $Fe_2(MoO_4)_3$, previously.[11] In addition, surfactant-assisted hydrothermal synthesis of nearly monodisperse MWO_4 (M = Pb, Ca) microspheres have also been demonstrated.[12] Nanorod or nanowire-guided self-aggregation of tiny nanoparticles in the case of $ZnWO_4$[13] and $ZnWO_4$@MWO_4 (M = Mn, Fe) were also reported.[14] The solution synthesis of metal molybdates includes $CaMoO_4$, $SrMoO_4$,[15] and lanthanum molybdate nanoflakes.[16] The catalytic and magnetic properties of these molybdates have been reported.[1,2,17] To our best knowledge, synthesis and phase control of a family of transition metal molybdate hydrates $MMoO_4 \cdot nH_2O$ (M = Co, Ni, Mn) by a solution strategy have not been demonstrated.

In this paper, we report systematically on how to selectively synthesize a family of transition metal molybdate hydrates $MMoO_4 \cdot nH_2O$ (M = Co, Ni, Mn) with well defined nano/microstructures and high yield by a simple hydrothermal approach. The influence of pH, reaction time, temperature, growth mechanism, and surfactant on the phase transformation, and sizes was discussed. Moreover, the photocatalytic, electrochemical, and magnetic property of these compounds has been investigated.

2. Experimental Section

2.1. Materials and Preparation. Polyethylene glycol (PEG-400, Mw = 380−430) in chemical grade was purchased from Shanghai Chem. Ltd. All other chemicals are analytical grade and used as received without further purification. In a typical procedure, 0.014 mmol of $(NH_4)_6Mo_7O_{24}$ was dissolved in 13 mL of distilled water, and 1 mmol of $M(NO_3)_2$ or MCl_2 (M = Co, Ni, Mn) was dissolved in 13 mL of deionized water, respectively (the mole ratio of Mo to metal is 1.0). Then, the $(NH_4)_6Mo_7O_{24}$ solution was slowly added into the $M(NO_3)_2$ or MCl_2 solution under magnetic stirring to form a homogeneous solution at room temperature. The pH was adjusted to a specific value using $NH_3 \cdot H_2O$ (25 wt %) or HNO_3 (1 mol L^{-1}) solution. The resulting precursor solution was transferred into a Teflon-lined stainless autoclave. The autoclave was sealed and maintained at 140 °C for 12 h, then allowed to cool to room temperature in air. After the reaction, the solution was filtered, washed by deionized water and absolute ethanol, respectively, and dried in a vacuum at 80 °C for 6 h.

2.2. Characterization. X-ray powder diffraction patterns (XRD) of the products were obtained on a Japan Rigaku DMax-γA rotation anode X-ray diffractometer equipped with graphite monochromatized Cu Kα radiation (λ = 1.54178 Å). The field-emission scanning electron microscope (FE-SEM) measurements were carried out with a field-emission microscope (JEOL, 7500B) operated at an acceleration voltage of 10 kV; transmission electron microscope (TEM) photographs were taken on a Hitachi Model H-800 transmission electron microscope at an accelerating voltage of 200 kV. High-resolution transmission electron microscope (HRTEM) photographs, and selected area electron diffraction (SAED) patterns were performed on a JEOL JEM 2011 microscope at an accelerating voltage of 200 kV.

Photocatalytic activities of the samples were evaluated by the photocatalytic decomposition of acid fuchsine under visible light. The photocatalytic reaction was carried out in a 25 mL glass bottle, which contained 20 mL of acid fuchsine solution (2.0×10^{-5} M), and 10 mg of the samples. The bottle was sealed and the mixture was allowed under 100 W UV light with continuous maganetic stirring. At given time intervals, 1 mL of the mixture solution was pipetted into a centrifugal-tube, for optical absorption measurements, the mixture solution was immediately centrifuged to remove the catalyst particles, which tend to scatter the incident beam. The centrifuged solution was then put into a quartz cell (path length 1.0 cm) and the absorption spectrum was measured with a Shimadzu UV 2550 ultraviolet−visible (UV−vis) spectrophotometer.

The magnetic properties of the obtained products were studied using a superconducting quantum interference device (SQUID, Quantum Design Corp., MPMS-XL, U.S.A.). Thermogravimetric analysis (TGA) was carried out on a TGA-50 thermal analyzer (Shimadzu Corporation) with a heating rate of 10 °C min^{-1} in flowing air. N_2 adsorption was determined by Brunauer−Emmett−Teller (BET) measurements using an ASAP-2000 surface area analyzer. Electrochemical tests were conducted with Teflon cells. The positive electrodes were fabricated by pasting slurries of the as-prepared $MMoO_4 \cdot nH_2O$ (M = Co, Ni, Mn) (85 wt %), carbon black (Super P, 10 wt %) and polyvinylidene (PVDF, 10 wt %) dissolved in N-methyl-pyrrolidinone (NMP) on Al foil strips by the doctor blade technique. Then the strips were dried at 140 °C for 24 h in an air oven, pressed under 20 Mpa pressures, and finally kept at 120 °C for 24 h in a vacuum. The electrolyte was 1 mol L^{-1} of $LiPF_6$ in a 1:1 mixture of ethylene carbonate (EC)/diethyl carbonate (DEC); the separator was Celgard 2500. Metallic lithium was used as negative electrode. The cells were assembled in the argon-filled glovebox with less than 5 ppm of water and oxygen. The cells were galvanostatically cycled in the 1.2−4.0 V range at a current density of 0.1 mA cm^{-2}.

3. Results and Discussion

3.1. General Synthesis of $MMoO_4 \cdot nH_2O$ (M = Co, Ni, Mn; n = 3/4, 1, 1). Hydrothermal treatment of an amorphous particulate dispersion made of $M(NO_3)_2$ (M = Co, Ni, Mn) and $(NH_4)_6Mo_7O_{24}$ at 140 °C for 12 h led to the formation of pure phase $MMoO_4 \cdot nH_2O$ (M = Co, Ni, Mn) with good crystallinity as shown in Figure 1; all reflection peaks of the different products prepared at pH 7 can be easily indexed as $CoMoO_4 \cdot 3/4H_2O$,[18] $NiMoO_4 \cdot H_2O$ (JCPDS Card No. 13−0128), and $MnMoO_4 \cdot H_2O$ (JCPDS Card No.: 78−0220), respectively.

(11) (a) Yu, S. H.; Liu, B.; Mo, M. S.; Huang, J. H.; Liu, X. M.; Qian, Y. T. *Adv. Funct. Mater.* **2003**, *13*, 639. (b) Cui, X. J.; Yu, S. H.; Li, L. L.; Liu, H. B.; Mo, M. S.; Liu, X. M. *Chem.—Eur. J.* **2004**, *10*, 218. (c) Ding, Y.; Yu, S. H.; Liu, C.; Zang, Z. A. *Chem.—Eur. J.* **2007**, *13*, 746.

(12) Zhang, Q.; Yao, W. T.; Chen, X. Y.; Zhu, L. W.; Fu, Y. B.; Zhang, G. B.; Yu, S. H. *Cryst. Growth Des.* **2007**, *7*, 1423.

(13) Liu, B.; Yu, S.; Li, L.; Zhang, F.; Zhang, Q.; Yoshimura, M.; Shen, P. *J. Phys. Chem. B* **2004**, *108*, 2788.

(14) Zhang, Q.; Chen, X. Y.; Zhou, Y. X.; Zhang, G. B.; Yu, S. H. *J. Phys. Chem. C.* **2007**, *111*, 3927.

(15) Chen, D.; Tang, K. B.; Li, F. Q.; Zheng, H. G. *Cryst. Growth. Des.* **2006**, *6*, 247.

(16) Xu, Y. P.; Jiang, D. Y.; Bu, W. B.; Shi, J. L. *Chem. Lett.* **2005**, *34*, 7.

(17) (a) Ehrenberg, H.; Svoboda, I.; Wltschek, G.; Wiesmann, M.; Trouw, F.; Weitzel, H.; Fuess, H. *J. Magn. Magn. Mater.* **1995**, *150*, 371. (b) Vie, D.; Martÿnez, E.; Sapin, F.; Folgado, J. V.; Beltrán, A. *Chem. Mater.* **2004**, *16*, 1697. (c) Ehnmberg, H.; Wltschek, G.; Knener, F. T. T.; Weitzel, H.; Fues, H. *J. Magn. Magn. Mater.* **1994**, *135*, 355.

(18) (a) Eda, K.; Uno, Y.; Nagai, N.; Sotani, N.; Whittingham, M. S. *J. Solid State Chem.* **2005**, *178*, 2791. (b) Eda, K.; Uno, Y.; Nagai, N.; Sotani, N.; Chen, C.; Whittingham, M. S. *J. Solid State Chem.* **2006**, *179*, 1453.

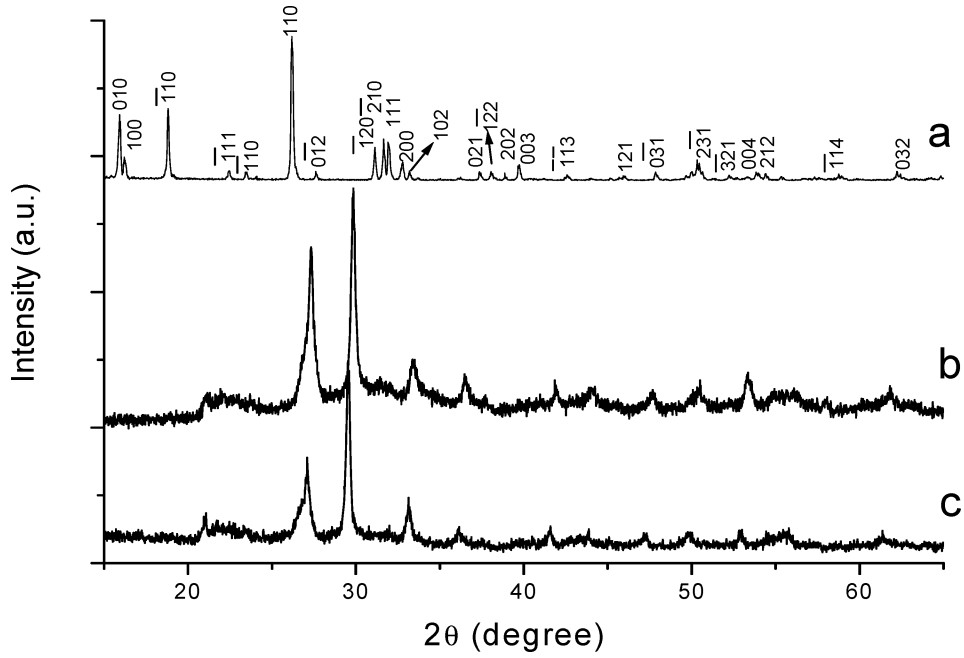

Figure 1. XRD pattern of the as-synthesized metal molybdate hydrates after reaction at 140 °C for 12 h, pH 7. (a) $MnMoO_4 \cdot H_2O$; (b) $NiMoO_4 \cdot H_2O$; (c) $CoMoO_4 \cdot 3/4H_2O$.

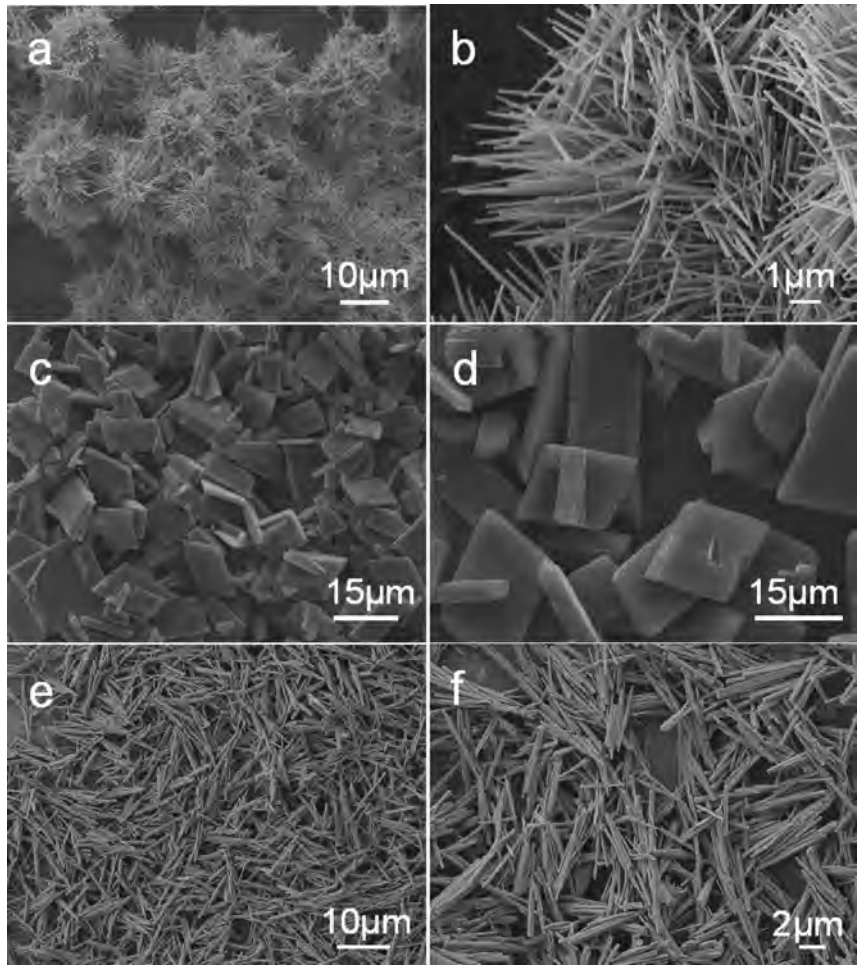

Figure 2. FE-SEM images of $MMoO_4 \cdot nH_2O$ (M = Co, Ni, Mn; n = 3/4, 1, 1) nanostructures and microstructures: (a, b) $NiMoO_4 \cdot H_2O$ microflowers, (c, d) $MnMoO_4 \cdot H_2O$ microparallelogram, (e, f) $CoMoO_4 \cdot 3/4H_2O$ microrods.

As shown in Figure 2, FE-SEM images of the $MMoO_4 \cdot nH_2O$ particles show different morphologies. Figure 2a shows that the product of $NiMoO_4 \cdot H_2O$ is in a form of microflowers with a diameter of about 20 μm, and each

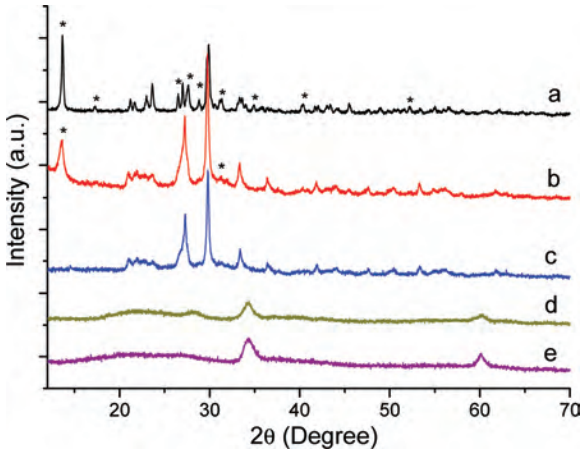

Figure 3. XRD patterns of the samples prepared at different pH values after reaction at 140 °C for 12 h. (a) pH 5, (b) pH 6, (c) pH 7, (d) pH 8, (e) pH 9. * donated $Ni_2(NO_3)_2(OH)_2 \cdot ?H_2O$.

Table 1. Influence of pH Value on the Phase of Metal Molybdate Hydrates

reaction system	pH	phase
$MnCl_2$ + $(NH_4)_6Mo_7O_{24}$	5	$(NH_4)_6MnMo_9O_{32}(H_2O)_6$ + $MnMoO_4 \cdot H_2O$
	7	$MnMoO_4 \cdot H_2O$
	9	$MnMoO_4 \cdot H_2O$ + $Mn_6O_{12} \cdot (H_2O)_{4.16}$
$Co(NO_3)_2$ + $(NH_4)_6Mo_7O_{24}$	5	$(NH_4)_4(CoMoH_6O_{24}) \cdot ?H_2O$ + $CoMoO_4 \cdot 3/4H_2O$
	7	$CoMoO_4 \cdot 3/4H_2O$
	9	$Co(OH)_2$
$Ni(NO_3)_2$ + $(NH_4)_6Mo_7O_{24}$	5	$NiMoO_4 \cdot H_2O$ + $Ni_2(NO_3)_2(OH)_2 \cdot ?H_2O$
	7	$NiMoO_4 \cdot H_2O$
	9	α-$3Ni(OH)_2 \cdot ?H_2O$

microflower is composed of packed nanowires with a diameter of about 130 nm as shown in a magnified SEM image in Figure 2b. The obtained $MnMoO_4 \cdot H_2O$ product consists of many microparallelogram plates, as clearly shown in Figures 2c,d. Figures 2e,f show that the obtained $CoMoO_4 \cdot 3/4H_2O$ is composed of microrods with the width of about 300 nm and the length of several micrometers.

The pH of the precursor solution has a crucial effect on both the formation of the molybdate phase and the morphology in the synthetic process. The controlled experiments were carried out to investigate the influence of pH on the synthesis of $NiMoO_4 \cdot H_2O$ microflowers and the phase evolution. When only $Ni(NO_3)_2$ and $(NH_4)_6Mo_7O_{24}$ solutions were mixed and its final pH was kept at 4.5, no product was obtained after hydrothermal treatment at 140 °C for 12 h. When the solution pH was adjusted to 5 with ammonia solution (25 wt %), a mixture of $NiMoO_4 \cdot H_2O$ and $Ni_2(NO_3)_2(OH)_2 \cdot ?H_2O$ (JCPDS Card No.: 27−0939) was obtained. If the pH of the solution was kept at 6, the main product is $NiMoO_4 \cdot H_2O$ and a little amount of $Ni_2(NO_3)_2(OH)_2 \cdot ?H_2O$ exists. If the pH value increases to 7, the product is pure $NiMoO_4 \cdot H_2O$ with flower-like structures. When pH is adjusted to 8 even 9, a green product α-$3Ni(OH)_2 \cdot ?H_2O$ (JCPDS Card No.: 22−0444) was observed. All XRD patterns of samples obtained at different pH are shown in Figure 3.

The above results suggest that the formation of $NiMoO_4 \cdot H_2O$ phase strongly depends on the initial pH of the dispersion. Similar results were also observed for the synthesis of $CoMoO_4 \cdot H_2O$ and $MnMoO_4 \cdot H_2O$. The phase formation zone can be mapped, as shown in Table 1. In addition, the temperature also has a significant influence on the formation of metal molybdate. The results show that the yield at low temperature, as low as 100 °C, under identical reaction conditions, is lower. When the temperature increases up to as high as 200 °C, the growth of the crystal is so rapid that the particle size increases dramatically.

The present system is a typical hydrothermal crystallization and ripening process. Here, the formation mechanism and shape evolution process of $NiMoO_4 \cdot H_2O$ has been carefully investigated (Scheme 1). Direct mixing of $(NH_4)_6Mo_7O_{24}$ solution and $Ni(NO_3)_2$ solution results in the formation of a transparent and green solution. With the pH value of solution changed from 4.5 to 7, the color is altered slightly but tiny nanoparticles appeared (Figure 4a). The electron diffraction (ED) pattern (inset in Figure 4a) shows that the particle is amorphous. After the solution with pH value of 7 aged at 140 °C for 3 h, aggregated particles and some urchin-like particles made of nanorods appeared (Figure 4b). After aging for 12 h, most of the particles are urchin-like (Figure 4c). When the aging time increased to 18 h, some wires fell off from the flower body (Figure 4d). When the two kinds of solutions are mixed, a highly supersaturated solution is adopted, and amorphous fine particles as the precursor will form immediately. The formation of tiny crystalline nuclei in supersaturated medium occurred at first and then it is followed by crystallization. The larger particles grow at the cost of the smaller ones because of the difference in solubility between the larger particles and the smaller particles, according to the well-known Gibbs−Thomson law.[19] The formation of nanorods/microrods of metal molybdate hydrate is possibly relative to the intrinsic crystal structure; reaction conditions are as for the hydrothermal synthesis of a family of metal tungstates nanorods reported previously.[11a,b]

3.2. General Synthesis of $MMoO_4 \cdot nH_2O$ in the Presence of PEG-400 (M = Co, Ni, Mn, n = 0, 3/4, 1). To change the sizes and microstructures of metal molybdate, a surfactant PEG-400 was added to the reaction solution. The

Scheme 1. Schematic Illustration of the Formation Process of Urchin-Like $NiMoO_4 \cdot H_2O$ Particles

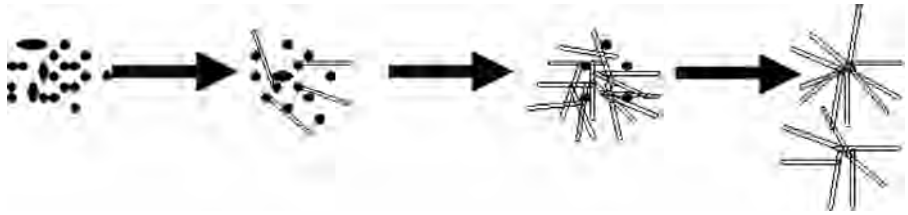

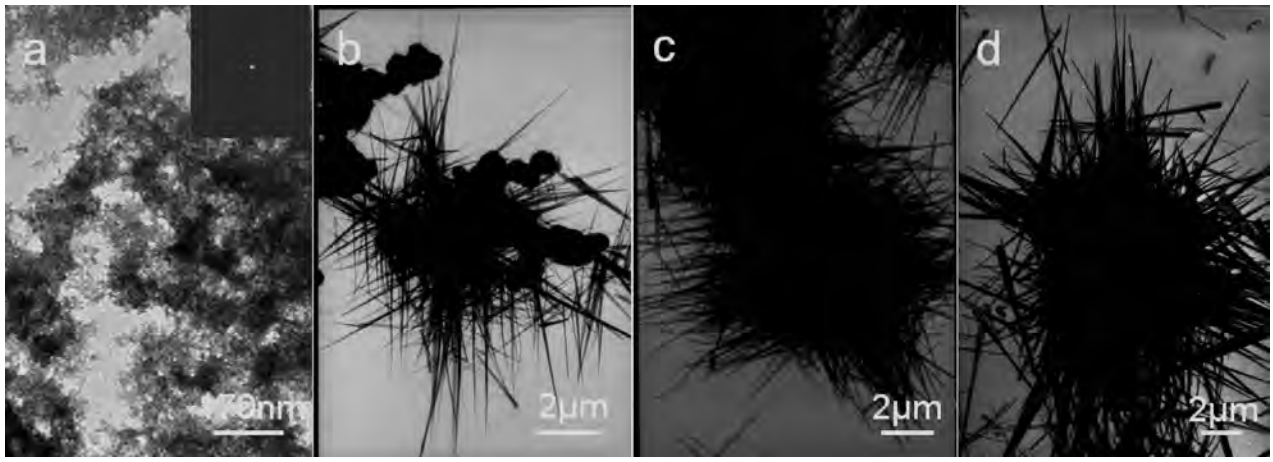

Figure 4. TEM images of the $NiMoO_4 \cdot H_2O$ particles prepared after different reaction stages. (a) Before hydrothermal reaction, inset shows its corresponding ED pattern; (b)−(d) after hydrothermal reaction for (b) 3 h, (c) 12 h, and (d) 18 h, respectively.

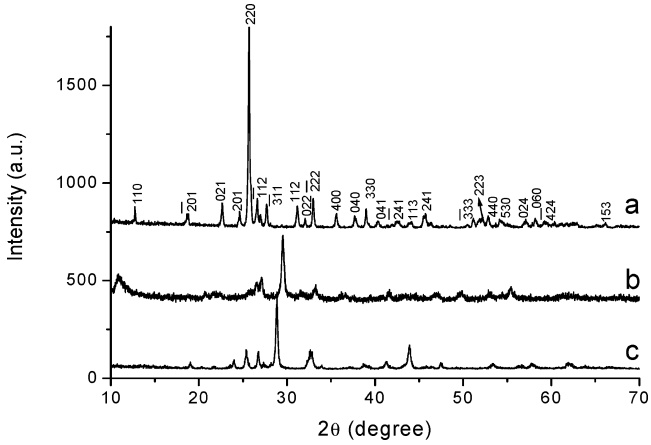

Figure 5. XRD patterns of the as-synthesized metal molybdate hydrates prepared in the presence of PEG-400, at 140 °C for 12 h, pH 7. (a) α-$MnMoO_4$, V_{PEG}/V_{water} = 2:1, (b) $CoMoO_4 \cdot 3/4H_2O$, V_{PEG}/V_{water} = 1:1, and (c) $NiMoO_4 \cdot H_2O$, V_{PEG}/V_{water} = 1:1.

results showed that PEG-400 played an important role in the formation of different morphologies of tungstate and molybdates, such as $MnWO_4$ and $PbMoO_4$ crystals under hydrothermal conditions.[20] Hydrothermal treatment of an amorphous particulate suspension with a pH value of 7 of $M(NO_3)_2$ (M = Co, Ni, Mn) and $(NH_4)_6Mo_7O_{24}$ in the presence of PEG-400 as surfactant at 140 °C for 12 h led to the formation of pure phase $MMoO_4 \cdot nH_2O$ (M = Co, Ni, Mn; n = 0, 3/4, 1) with good crystallinity, as shown in Figure 5. All reflection peaks of the different samples prepared at pH 7 can be easily indexed as the phase for purple $CoMoO_4 \cdot 3/4H_2O$ that was reported in 2005,[18] light yellow $NiMoO_4 \cdot H_2O$ (JCPDS Card No.: 13−0128), and white monoclinic α-$MnMoO_4$ with a = 10.46, b = 9.52, c = 7.14, β = 106.28 (JCPDS Card No. 72−0285), respectively (Figure 5).

The volume ratio of PEG-400 to water has significant influences on the phases and morphology of metal molybdate hydrates and metal molybdates. The selective phase synthesis of the products in the presence of PEG-400 at pH 7, at 140 °C for 12 h, is clearly shown in Table 2. $MnMoO_4 \cdot H_2O$ and α-$MnMoO_4$ phases were selectively synthesized when the volume ratio of V_{PEG}/V_{water} is lower than 2 or higher than

Table 2. Effect of the Volume Ratio of PEG-400 to Water (V_{PEG}/V_{water}) on the Phase of Metal Molybdates

reactants	V_{PEG}/V_{water}	phase
$MnCl_2$ + $(NH_4)_6Mo_7O_{24}$	<2	$MnMoO_4 \cdot H_2O$
	≥2	α-$MnMoO_4$
$Co(NO_3)_2$ + $(NH_4)_6Mo_7O_{24}$	≤2	$CoMoO_4 \cdot 3/4H_2O$
	>2	$(NH_4)_4(CoMoH_6O_{24}) \cdot ?H_2O + CoMoO_4 \cdot 3/4H_2O$
$Ni(NO_3)_2$ + $(NH_4)_6Mo_7O_{24}$	≤2	$NiMoO_4 \cdot H_2O$
	>2	$Ni_2(NO_3)_2(OH)_2 \cdot ?H_2O + NiMoO_4 \cdot H_2O$

or equal to 2, respectively. $CoMoO_4 \cdot 3/4H_2O$ and $NiMoO_4 \cdot H_2O$ were obtained when the volume ratio of V_{PEG}/V_{water} is lower than 2 or equal to 2, respectively.

FE-SEM images in Figure 6 show the different morphologies of $MMoO_4 \cdot nH_2O$ (n = 0, 3/4, 1) particles. Figure 6a,b shows that the obtained $CoMoO_4 \cdot 3/4H_2O$ particles are nanorod-like and have an average diameter of 150 nm and lengths of 2 μm. Similar rod-like $NiMoO_4 \cdot H_2O$ particles are observed and they have a diameter of 100 nm and lengths of 1.2 μm as shown in Figure 6c,d. α-$MnMoO_4$ particles are in form of elongated microrods with a diameter of 1 μm and lengths up to 20 μm as shown in Figure 6e,f. The $NiMoO_4 \cdot H_2O$ particles are nanobundles, each rod is composed of several nanorods in a way of oriented attachment with each other and have a diameter of about 20 nm (see Supporting Information, Figure S1).

The formation of $MMoO_4 \cdot nH_2O$ (M = Co, Ni, n = 3/4, 1) nanorod bundles can be explained by an aggregation based growth process under hydrothermal conditions. The detailed formation process of $NiMoO_4 \cdot H_2O$ nanorod bundles has been followed. At the very beginning, solutes are formed to yield a supersaturated solution, leading to nucleation and the formation of amorphous tiny nanoparticles (see Supporting Information, Figure S2a). After reaction for 1 h, most of particles grew into rods accompanied with amorphous particles still (see Supporting Information, Figure S2b). When the reaction time was longer than 6 h, the uniform nanorod bundles were obtained (see Supporting Information, Figure S2c,d). The tendency for aggregation of nanorods is to eliminate the surface energy, which is similar to the SnO_2

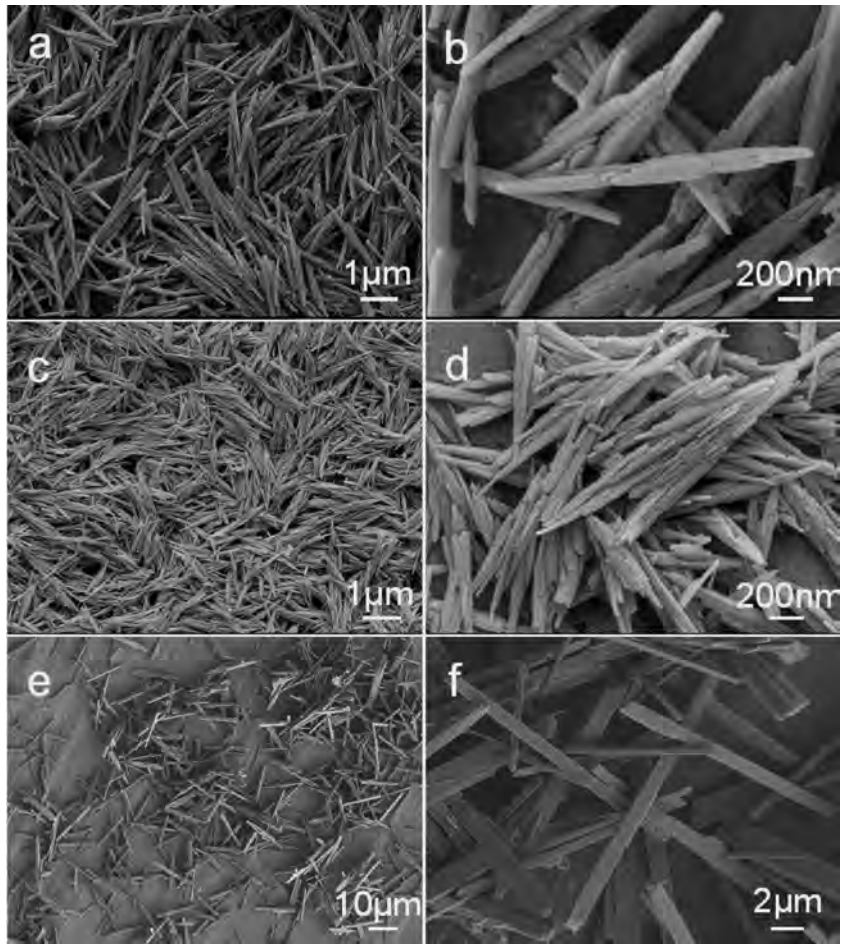

Figure 6. FE-SEM images of $MMoO_4 \cdot nH_2O$ (M = Co, Ni, Mn) particles synthesized under different conditions. (a, b) $CoMoO_4 \cdot 3/4H_2O$ nanorod bundles, V_{PEG}/V_{water} = 1:1. (c, d) $NiMoO_4 \cdot H_2O$ nanorod bundles, V_{PEG}/V_{water} = 1:1. (e, f) α-$MnMoO_4$ microrods, V_{PEG}/V_{water} = 2:1.140 °C, pH 7, 12 h.

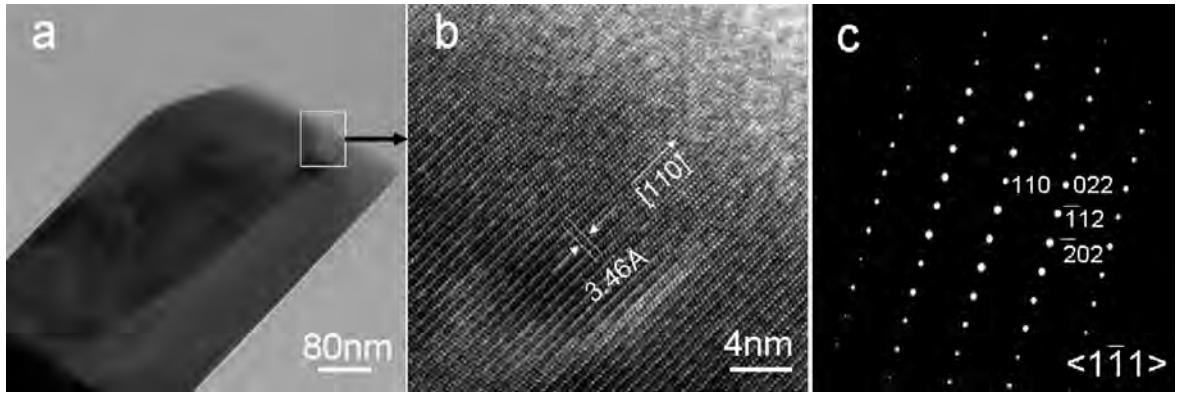

Figure 7. (a) TEM image, (b) HRTEM image, and (c) ED pattern for a typical α-$MnMoO_4$ nanorod.

nanorods in a solvothermal colloid system[21] and $In(OH)_3$ nanorod bundles observed in a microemulsion-mediated hydrothermal system.[22]

Figure 7a shows a TEM image of an individual α-$MnMoO_4$ rod. The crystal structure and growth orientation of an individual rod was examined by the HRTEM and SAED pattern. Figure 7b presents a representative HRTEM image of this rod, the well-resolved lattice planes demonstrate that each rod is single crystalline. The measured interplanar spacing is about 3.46 Å, corresponding to that of {110} planes of monoclinic phase α-$MnMoO_4$. The SAED pattern shown in Figure 7c taken from one individual rod can be indexed for the [1$\bar{1}$1] zone axis of α-$MnMoO_4$, in which diffraction spots can be clearly seen and reveal the single crystalline nature of the rod. The HRTEM image and SAED pattern indicate that the growth direction of rods is along [110].

(19) Madras, G.; Mccoy, B. J. *Chem. Eng. Sci.* **2002**, *57*, 3809.
(20) (a) Chen, S. J.; Chen, X. T.; Xue, Z. L.; Zhou, J. H.; L, J.; Hong, J. M.; You, X. Z. *J. Mater. Chem.* **2003**, *13*, 1132. (b) Cheng, Y.; Wang, Y. S.; Chen, D. Q.; Bao, F. *J. Phys. Chem. B* **2005**, *109*, 794.
(21) Zhang, D. F.; Sun, L. D.; Yin, J. L.; Yan, C. H. *Adv. Mater.* **2003**, *15*, 1022.

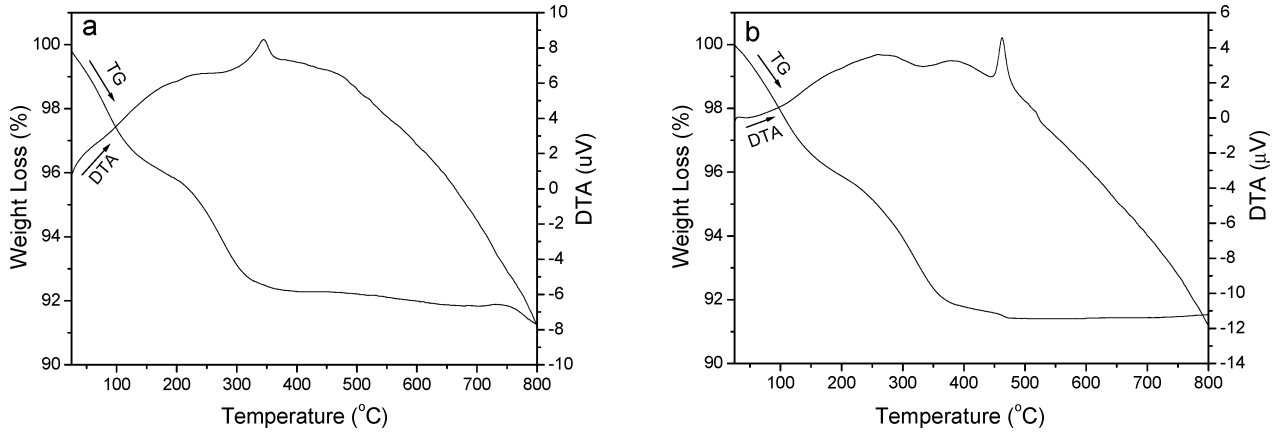

Figure 8. TGA and DTA curves of the prepared molybdate hydrates synthesized in the presence of PEG-400, pH 7, 140 °C, V_{PEG}/V_{water} = 1:1. (a) $CoMoO_4 \cdot 3/4H_2O$ and (b) $NiMoO_4 \cdot H_2O$.

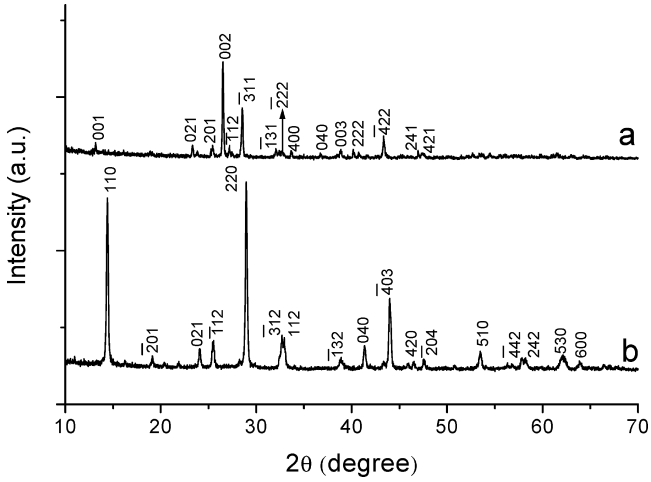

Figure 9. XRD patterns of the obtained metal molybdates after calcination of $CoMoO_4 \cdot 3/4H_2O$ and $NiMoO_4 \cdot H_2O$ at 500 and 550 °C, respectively. (a) β-$CoMoO_4$ and (b) α-$NiMoO_4$. The $CoMoO_4 \cdot 3/4H_2O$ and $NiMoO_4 \cdot H_2O$ samples were synthesized in the presence of PEG-400, pH 7, 140 °C, V_{PEG}/V_{water} = 1:1.

3.3. Thermal Stability Of $CoMoO_4 \cdot 3/4H_2O$ and $NiMoO_4 \cdot H_2O$ Synthesized in the Presence of PEG-400. TGA curves of the $CoMoO_4 \cdot 3/4H_2O$ and $NiMoO_4 \cdot H_2O$ samples with the temperature ranging from 30 to 800 °C show that net weight loss for $CoMoO_4 \cdot 3/4H_2O$ occurred at about 450 °C and for $NiMoO_4 \cdot H_2O$ at 500 °C is 5.5 wt % and 6.4 wt %, respectively (Figure 8). This weight loss is greatly ascribed to the loss of water, corresponding to water content in the produced $CoMoO_4 \cdot 3/4H_2O$ and $NiMoO_4 \cdot H_2O$, respectively. To obtain $CoMoO_4$ and $NiMoO_4$, the samples $CoMoO_4 \cdot 3/4H_2O$ and $NiMoO_4 \cdot H_2O$ were calcined at 500 and 550 °C, respectively. All the peaks in the XRD patterns shown in Figure 9 for the calcined products can be indexed to pure monoclinic β-$CoMoO_4$ with a = 10.2, b = 9.27, c = 7.02, β = 106.9° (JCPDS Card No.: 21−0868) and α-$NiMoO_4$ (a = 9.546, b = 8.73, c = 7.65, β = 114.2° (JCPDS Card No.: 86−0361).

The crystal structure and orientation of the obtained β-$CoMoO_4$ rods by calcination at 500 °C have been characterized by high resolution TEM and SAED patterns. The rod-like morphology of β-$CoMoO_4$ was still maintained after calcination, as clearly shown in Figure 10a. The SAED pattern in Figure 10b taken from one individual rod can be indexed as a [11$\bar{2}$] zone axis of α-$CoMoO_4$, showing the single crystalline nature of the rod. Figure 10c presents a representative HRTEM image of the same rod, the well-resolved lattice planes demonstrate that the wires are single crystalline. The lattice spacings along the different directions can be determined as 3.49 and 3.81 Å, corresponding to the interplanar spacings of the (201) and (021) planes for β-$CoMoO_4$, respectively.

3.4. Photoreductive Activity and Electrochemical Property. The BET surface area data for different calcined metal molybdates samples are summarized in Table 3. The BET surface area of nickel molybdate is slightly smaller than that reported in the literature but that of cobalt molybdate is slightly larger.[23] It is well-known that $MMoO_4$ (M = Co, Ni, Mn) has been used for oxidative dehydrogenation of butane and propane, and so forth;[24] however, these compounds have never been used to photodegrade water pollutants as Bi_2MoO_6 did.[25]

To demonstrate the potential applications of as-synthesized metal molybdates $CoMoO_4$ and $NiMoO_4$ nanorod bundles, which were calcined from the samples $CoMoO_4 \cdot 3/4H_2O$ and $NiMoO_4 \cdot H_2O$ prepared in the presence of PEG-400, and $MnMoO_4$ microrods, their photocatalytic activities have been investigated by choosing the photocatalytic degradation of acid fuchsine as a model reaction. The characteristic absorption of acid fuchsine at about 543 nm was chosen as the monitored parameter for the photocatalytic degradation process. Figure 11 shows the absorption spectra of an aqueous

(22) Yang, J.; Lin, C. K.; Wang, Z. L.; Lin, J. *Inorg. Chem.* **2006**, *45*, 8973.
(23) (a) Brito, J. L.; Barbosa, A. L. *J. Catal.* **1997**, *161*, 467. (b) David, V.; Eduardo, M.; Fernando, S.; José, V. F.; Aurelio, B.; Rita, X. V.; Vicente, C. C. *Chem. Mater.* **2004**, *16*, 1697.
(24) (a) Rajaram, P.; Viswanathan, B.; Sastri, M. V. C.; Srinivasan, J. J. *J. Chem.* **1974**, *12*, 1267. (b) Veleva, S.; Frifiro, F. *React. Kinet. Catal. Lett.* **1976**, *4*, 19. (c) Burrington, J. D.; Grasselli, R. K. *J. Catal.* **1979**, *59*, 79. (d) Burrington, J. D.; Kartisek, C. T.; Grasselli, R. K. *J. Catal.* **1980**, *63*, 235. (e) Aranda, R. M. M.; Portela, M. F.; Madeira, L. M.; Freire, F.; Oliveira, M. *Appl. Catal., A: General* **1995**, *127*, 201. (f) José, A. R.; Sanjay, C.; Jonathan, C. H.; Alberto, A.; Joaquín, L. B. *J. Phys. Chem. B* **1998**, *102*, 1347. (g) José, A. R.; Sanjay, C.; Jonathan, C. H. *J. Phys. Chem. B* **1999**, *103*, 770.
(25) (a) Beale, A. M.; Sankar, G. *Chem. Mater.* **2003**, *15*, 146. (b) Yu, J. Q.; Kudo, A. *Chem. Lett.* **2005**, *34*, 1528.

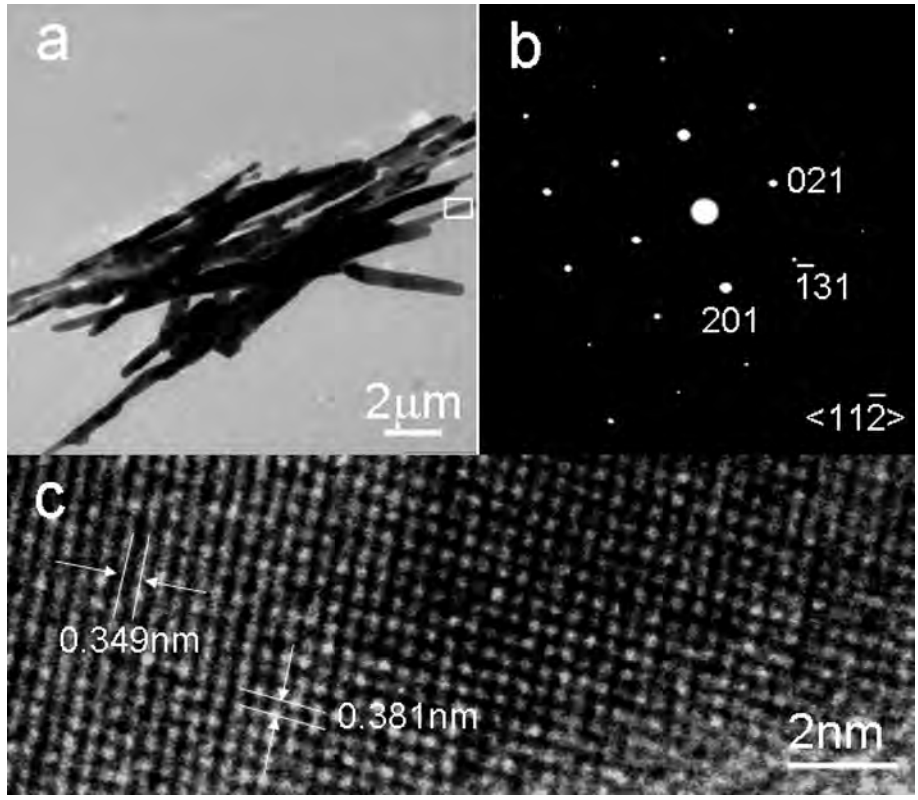

Figure 10. (a) TEM image, (b) the ED pattern, and (c) HRTEM image of an individual β-$CoMoO_4 \cdot 3/4H_2O$ rod synthesized after calcination of $CoMoO_4 \cdot 3/4H_2O$ at 500 °C for 2 h. The $CoMoO_4 \cdot 3/4H_2O$ sample was synthesized in the presence of PEG-400, pH 7, 140 °C, $V_{PEG}/V_{water} = 1{:}1$.

Table 3. BET Surface Area for Different Metal Molybdates Products

as-prepared products	BET surface area (m^2/g)
$NiMoO_4 \cdot H_2O$	31
$CoMoO_4 \cdot 3/4H_2O$	25
α-$NiMoO_4$ (calcined)	29
β-$CoMoO_4$ (calcined)	24
α-$MnMoO_4$	15

solution of acid fuchsine (initial concentration, 2.0×10^{-5} M, 20 mL) in the presence of 10 mg of metal molybdate samples prepared under the same conditions under exposure to UV light for 30 min. The intensity of the absorption peaks corresponding to the acid fuchsine, such as the sharp peak at 543 nm, decreased as the photocatalytic reaction time increased. No new absorption bands appeared in either visible or ultraviolet regions, suggesting the complete photodegradation of the acid fuchsine. The results indicate that the photocatalytic activity of the prepared $CoMoO_4$ nanorod bundles show highest photocatalytic capability among the three samples obtained in the present reaction system (Figure 11d).

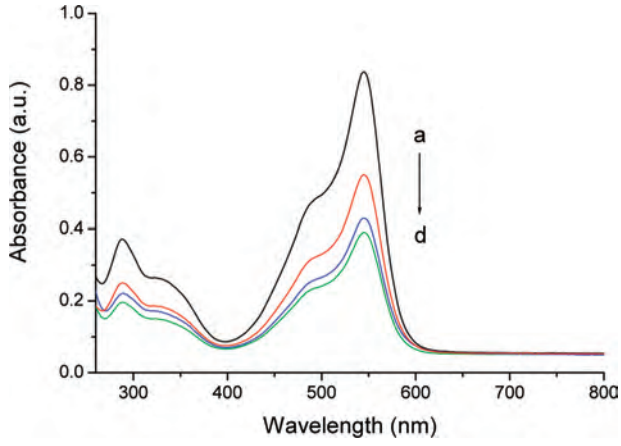

Figure 11. Absorption spectra of a solution of acid fuchsine (2×10^{-5} M, 20 mL) in the presence of metal molybdates particles (10 mg) under exposure to UV light for 30 min. (a) Initial acid fuchsine solution; (b−d) corresponding to the spectra measured after adding the prepared samples (b) $NiMoO_4$, (c) $MnMoO_4$, and (d) $CoMoO_4$.

To understand the potential advantage of $CoMoO_4$ nanorod bundles as photocatalyst for photodegradation of acid fuchsine, time-dependent UV−vis absorption spectra of the solution with initial concentration of 2.0×10^{-5} M (20 mL) acid fuchsine were recorded. As shown in Figure 12, the peaks of acid fuchsine gradually weakened and the color of the solution gradually lightened as the exposure time extended in the presence of 10 mg of $CoMoO_4$ nanorod bundles. During this process, the typical sharp peak at 543 nm diminished and faded nearly completely with the exposure time increasing to 180 min.

The electrochemical performance of $MMoO_4$ (M = Ni, Co) nanorod bundles and $MnMoO_4$ microrods has been evaluated too. $MMoO_4$ (M = Ni, Co) nanorod bundles were obtained from calcination of $CoMoO_4 \cdot 3/4H_2O$ and $NiMoO_4 \cdot H_2O$, at 500 and 550 °C, respectively. The $CoMoO_4 \cdot 3/4H_2O$ and $NiMoO_4 \cdot H_2O$ nanorod bundles were prepared by a hydrothermal process at pH 7, 140 °C, $V_{PEG}/V_{water} = 1{:}1$, and the $MnMoO_4$ microrods were obtained at pH 7, 140 °C, $V_{PEG}/V_{water} = 2{:}1$. Figure 13 show the voltage versus capacity for the cells between 1.2 and 4.0 V at a current density of 0.1 mA cm^{-2}. Obviously, the first

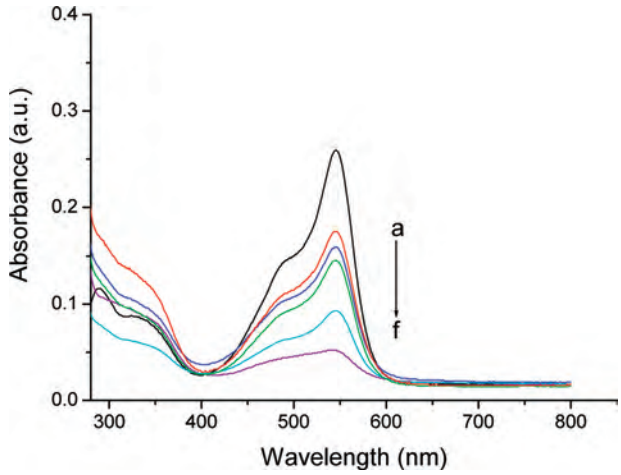

Figure 12. Time-dependent absorption spectra of a solution of acid fuchsine (7×10^{-6} M, 20 mL) in the presence of 10 mg of $CoMoO_4$ nanorod bundles after its exposure to UV light. (a) Initial solution; (b−f) after exposure to UV light for (b) 15, (c) 30, (d) 60, (e) 120, and (f) 180 min.

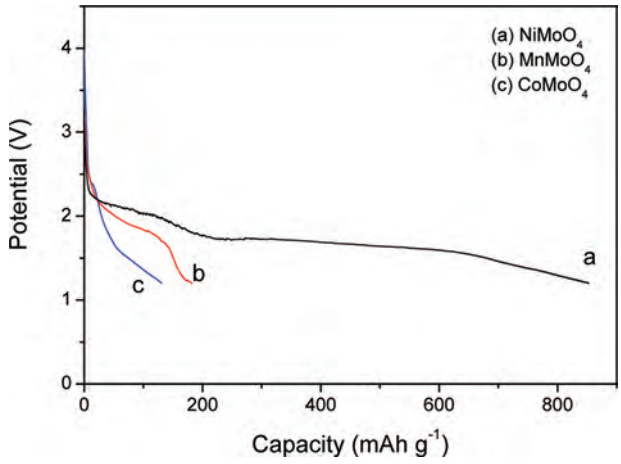

Figure 13. First discharge−charge curve of the as-prepared $MMoO_4$ (M = Mn, Ni, Co). (a) $NiMoO_4$, (b) $MnMoO_4$, (c) $CoMoO_4$. The cells were galvanostatically cycled in the 1.2−4.0 V range at a current density of 0.1 mA cm^{-2}.

discharge capacity of the $NiMoO_4$ is the best and it can reach 850 mA h g^{-1}. The discharge curves have the clear voltage plateaus around 1.8 V. It is much better than that for $CoMoO_4$ (130 mA h g^{-1}) and $MnMoO_4$ (180 mA h g^{-1}), and the value is better than that reported for the first discharge capacity of the $NiMoO_4$.[26] It is proposed that such a high capacity is related to many vacancies in the structure of $NiMoO_4$ nanorod bundles, in which Li^+ ion could be reversibly incorporated.

3.5. Magnetic Property. $MMoO_4 \cdot nH_2O$ (M = Co, Ni, Mn; n = 0, 3/4, 1) has an interesting magnetic property. $MnMoO_4$ has three polymorphs: α-$MnMoO_4$,[27] another phase of $MnMoO_4$, wolframite structure (W-$MnMoO_4$), obtained from the reaction of MnO with MoO_3 at high pressure (60 kbar) and high temperature (900 °C).[28] In the third structure of $MnMoO_4$, different from α-$MnMoO_4$, in which the Mo atom has a somewhat distorted tetrahedral coordination, the Mo atom is in a highly distorted octahedral coordination.[6] Corbet et al.[29] and Sinhamahapatra et al.[30] obtained $MnMoO_4 \cdot 0.9H_2O$ and $MnMoO_4 \cdot 1.5H_2O$, respectively. To the best of our knowledge, the magnetic properties of $MnMoO_4 \cdot H_2O$ and α-$MnMoO_4$ have not been studied so far. The magnetism of $MnMoO_4 \cdot H_2O$ and α-$MnMoO_4$ were measured in the temperature range between 4 and 150 K using a SQUID (Quantum Design) magnetometer with a 100 G field strength. The temperature dependence of the magnetization and the $\chi_m T$ product of $MnMoO_4 \cdot H_2O$ and α-$MnMoO_4$ are shown in Figure 14. Antiferromagnetic ordering is observed at about 12 K for both $MnMoO_4 \cdot H_2O$ and $MnMoO_4$; at higher temperatures they begin to follow the Curie−Weiss law. The curve fitting between 80 and 150 K gives a negative Curie−Weiss temperature $\theta = -36.6$ and −37.2 K, respectively.

Four compounds with the $CoMoO_4$ stoichiometry are known: the low temperature α-phase (pale green),[31] the high temperature β-phase (pale violet),[26] the high-pressure (hp-) phase (black),[2] and the hydrate ($CoMoO_4 \cdot 3/4H_2O$).[18] To our best knowledge, the magnetic property of $CoMoO_4 \cdot 3/4H_2O$ has not been studied yet. Magnetization of $CoMoO_4 \cdot 3/4H_2O$ was measured in the temperature range between 4 and 250 K using a SQUID (Quantum Design) magnetometer with a 5000 G field strength. The temperature dependence of the magnetization and the $\chi_m T$ product of $CoMoO_4 \cdot 3/4H_2O$ are shown in Figure 15 where antiferromagnetic ordering observed at about 9 K is much lower than that at 48 K measured by Livage et al.,[2] which is a high pressure phase. At higher temperatures, $CoMoO_4 \cdot 3/4H_2O$ begins to follow the Curie−Weiss law. The curve fits between 180 and 300 K give a Curie−Weiss temperature $\theta = -14.7$ K.

The obtained α-$NiMoO_4$ and $NiMoO_4 \cdot H_2O$ after calcination show similar magnetic properties. Figure 16 shows magnetic properties of the microflowers of $NiMoO_4 \cdot H_2O$ (Ni1) synthesized without adding PEG-400, with PEG-400 (Ni2), and the obtained α-$NiMoO_4$ (Ni3) by calcination of the sample Ni2 at 550 °C for 2 h, respectively. Their magnetic properties are similar to that of α-$NiMoO_4$, as measured by Ehrenberg et al.[17a] Here, magnetization of the samples Ni1, Ni2, and Ni3 was measured in the temperature range between 4 and 160 K using a SQUID (Quantum Design) magnetometer with a 100 G field strength. The curve fits between 100 and 160 K give Curie−Weiss temperatures of θ = 20.5, 23.3, and 18.0 K, respectively. The antiferromagnetic component is determined to be 3.66, 3.19, and 3.23 μ_B, respectively, per Ni-ion at 160 K, based on the zero field magnetization obtained by linear extrapolation of the high-temperature behavior.

(26) Leyzerovich, N. N.; Bramnik, K. G.; Buhrmester, T.; Ehrenberg, H.; Fuess, H. *J. Power Sources* **2004**, *127*, 76.
(27) Sleight, A. W.; Chamberland, B. I. *Inorg. Chem.* **1968**, *7*, 1672.
(28) Abrahams, S. C.; Reddy, J. M. *J. Chem. Phys.* **1965**, *43*, 2533.
(29) Corbet, F.; Eyraud, C. *Bull. Soc. Chim. Fr.* **1961**, 571.
(30) Sinhamahapatra, P. K.; Bhattacharyya, S. K. *J. Therm. Anal.* **1975**, *8*, 45.
(31) Smith, G. M.; Ibers, J. A. *Acta. Crystallogr.* **1965**, *19*, 269.

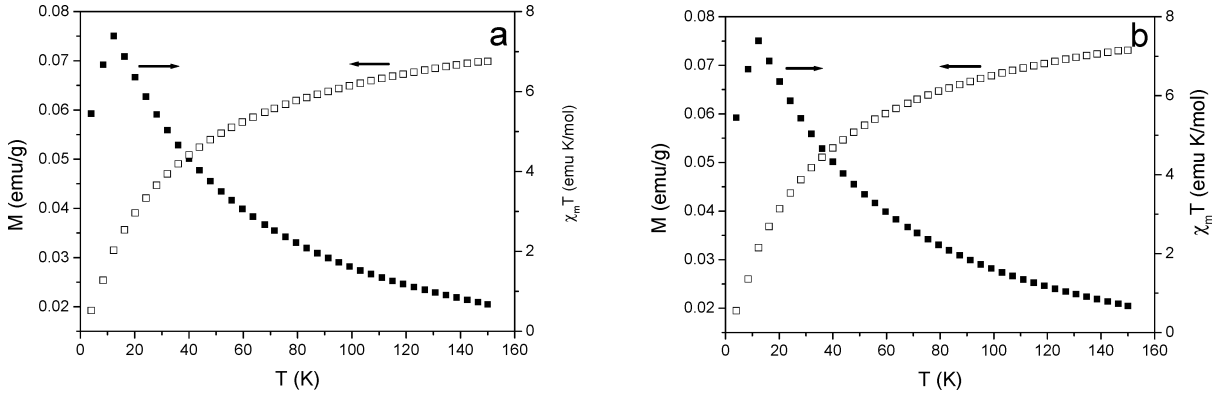

Figure 14. Temperature dependence of magnetization and $\chi_m T$ of (a) $MnMoO_4 \cdot H_2O$, 140 °C, 12 h, pH 7, and (b) α-$MnMoO_4$, 140 °C, 12 h, pH 7, $V_{PEG}/V_{water} = 2:1$.

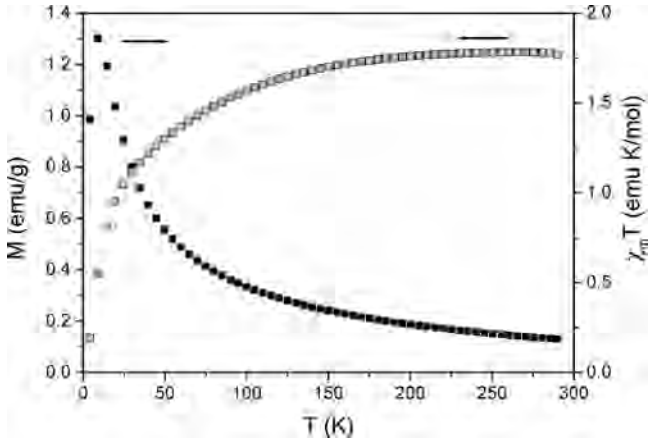

Figure 15. Temperature dependence of magnetization and $\chi_m T$ of $CoMoO_4 \cdot 3/4H_2O$, synthesized at 140 °C for 12 h, pH 7, $V_{PEG}/V_{water} = 1:1$.

4. Conclusion

In conclusion, a family of molybdate hydrates $MMoO_4 \cdot nH_2O$ (M = Co, Ni, Mn, n = 0, 3/4, 1) nano/microcrystals can be selectively synthesized by a hydrothermal process. With addition of PEG-400, uniform nanorod bundles of $NiMoO_4 \cdot H_2O$ and $CoMoO_4 \cdot 3/4H_2O$ can be obtained. Particularly, microrods of α-$MnMoO_4$ can be synthesized by adjusting the volume ratio of PEG-400 to water. The calcination of $CoMoO_4 \cdot 3/4H_2O$ and $NiMoO_4 \cdot H_2O$ at 500 and 550 °C, respectively, allows the formation of monoclinic β-$CoMoO_4$ and α-$NiMoO_4$.

The photocatalytic activities of $CoMoO_4$ nanorod bundles, $NiMoO_4$ nanorod bundles, and $MnMoO_4$ microrods have been investigated by choosing the photocatalytic degradation of acid fuchsine as a test model. It is found that $CoMoO_4$ showed a high photocatalytic activity. The electrochemical performance of $MMoO_4$ (M = Ni, Co) nanorod bundles and $MnMoO_4$ microrods has been evaluated. The first reversible discharge specific capacity for $NiMoO_4$ can reach up to 850 mA h g^{-1} versus Li metal at 0.1 mA cm^{-2} (voltage range 1.2−4.0 V), which is higher than for $CoMoO_4$ (130 mA h g^{-1}) and for $MnMoO_4$ (180 mA h g^{-1}). Furthermore, the magnetic properties of $MnMoO_4 \cdot H_2O$, α-$MnMoO_4$, and $CoMoO_4 \cdot 3/4H_2O$ were measured and discussed for the first time. This family of transition metal molybdate hydrates $MMoO_4 \cdot nH_2O$ (M =

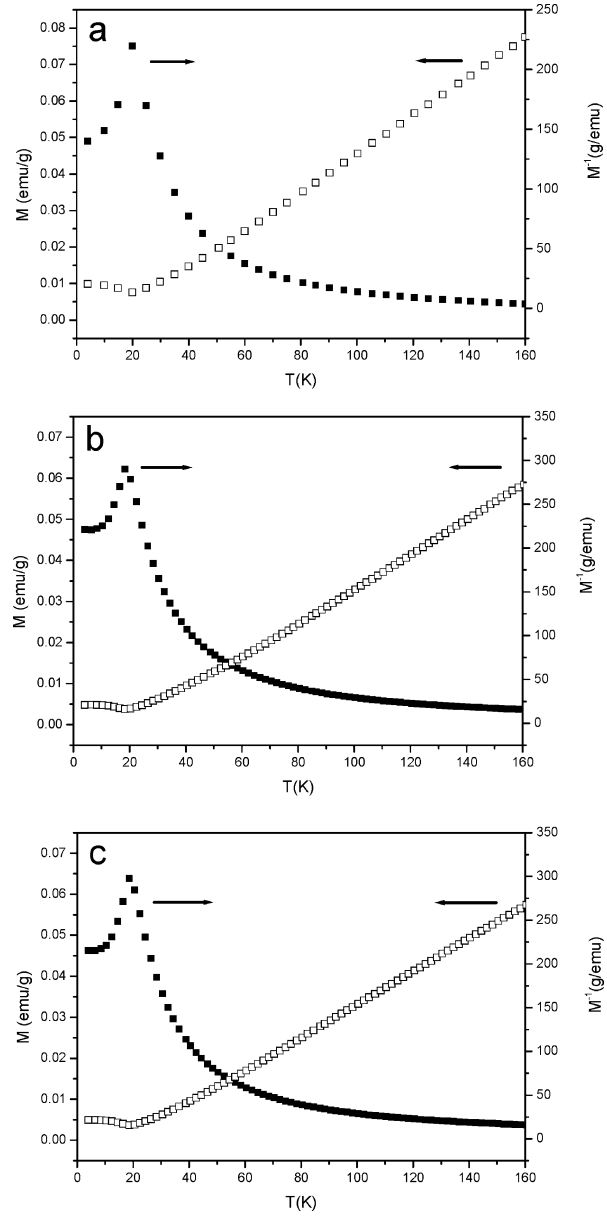

Figure 16. Temperature dependence of inverse magnetization and magnetization. (a) Ni1, the sample $NiMoO_4 \cdot H_2O$ was prepared at 140 °C for 12 h, pH 7, in the absence of PEG-400. (b) Ni2, the sample $NiMoO_4 \cdot H_2O$ was prepared at 140 °C for 12 h, pH 7, V_{PEG}/V_{water} = 1:1. (c) Ni3, the sample α-$NiMoO_4$ was prepared by calcination of the sample Ni2 at 550 °C for 2 h.

Co, Ni, Mn, $n = 0$, 3/4, 1) with interesting photocatalytic, electrochemical, and magnetic properties may find applications in the future.

Acknowledgment. S.H.Y. thanks the financial support from the Natural Science Foundation of China (Grants 50732006, 20325104, 20621061, 20671085), the 973 project (Grant 2005CB623601), Anhui Development Fund for Talent Personnel and Anhui Education Committee (2006Z027, ZD2007004-1), the Scientific Research Foundation for the Returned Overseas Chinese Scholars, the Specialized Research Fund for the Doctoral Program (SRFDP) of Higher Education State Education Ministry, and the Partner-Group of the Chinese Academy of Sciences-the Max Planck Society.

Supporting Information Available: Figures S1 and S2 containing TEM images. This material is available free of charge via the Internet at http://pubs.acs.org.

IC8007975